THE AFRICAN EQUATORIAL IONIZATION ANOMALY RESPONSE TO THE ST. PATRICK'S DAY STORMS OF MARCH 2013 AND 2015

Olawale S. Bolaji[2,3], Bolarinwa J. Adekoya[1*], Shola J. Adebiyi[4], Babatunde O. Adebesin[4], Stephen O. Ikubanni[4],

[1]*Department of Physics, Olabisi Onabanjo University, P.M.B. 2002, Ago Iwoye, Ogun State, Nigeria*

[2]*Department of Physics, University of Lagos, Akoka – Yaba, Lagos State, Nigeria*

[3]*Department of Physics, University of Tasmania, Hobart, Australia*

[4]*Space Weather Group, Department of Physical Sciences, Landmark University, P.M.B 1001, Omu-Aran, Kwara State, Nigeria*

[*]*Correspondence Author*: adekoyabolrinwa@yahoo.com; adekoya.bolarinwa@oouagoiwoye.edu.ng (+2347038124660; +2348155123736).

Abstract

The ionosphere around the Equatorial ionization Anomaly (EIA) region exhibits a complex dynamic and responds markedly to the solar-magnetospheric energy and momentum. In this paper, the hourly response of the EIA structure in the Africa to St. Patrick's Day storms of March 2013 and 2015 is investigated using data obtained from a chain of GPS receivers located in the African region. The TEC variations were characterized based on the convective magnetospheric dynamo fields, the neutral wind circulation, and zonal electric fields. Generally, the result indicates that the TEC variations were consistent with the different directions of the interplanetary fields during the different phases of the storms. We observed reverse EIA structures in the main phase of the storm of March 2015, suggests to be related to the intense PPEF and strong equatorward wind which imposed westward zonal electric field at the equator. Similar equatorial peak observed during the recovery phase is associated to DDEF, poleward wind and plasma convergence. Furthermore, TEC variations also indicate hemispheric asymmetries during the storms. During the main phase, the TEC is more enhanced in the northern hemisphere during the storm of March 2013, this was reversed during March 2015. We observed equatorial peak during SSC period of the storm of March 2013, while EIA structures are generally weak in March 2015 event. This may posit that ionospheric pre-storm behaviour is better understood when the IMF-Bz and electric field are weak. The observed distinctive response avowed the peculiarity in the electrodynamics intricacy in the Africa sector.

Keywords: EIA, TEC, Plasma reversal, DDEF, PPEF, Pre-Storm

Key Points

- The response of the EIA structure in the Africa to two St. Patrick's storm events of 2013 and 2015 was investigated
- The IMF-Bz and IEF changed the EIA structures on an hourly base during the two storms
- Plasma reversal was seen in the main phase during the March 2015 storm, an uncommon EIA structure
- The response of the EIA structure in both hemispheres to the two storms events differs
- Ionospheric pre-storm in the EIA region is better understood when Interplanetary fields are not significant.

1. Introduction

The stream of solar energetic particles emitted from the Sun towards the Earth's is a major space weather hazard and motivating the development of the ionospheric disturbances. The emitted charged particles cause the exchange of energy from the solar wind into the earth's environment and cause a temporary perturbation of the Earth's magnetic field, a phenomenon known as a geomagnetic storm. The convections of these charged corpuscles have easy access to the high latitude (where it is dissipated in the form of joules and particle heating) compared to other latitudes and are transported via the magnetic line of force into the polar region (Kamide, 1982; Baumjohann, 1982). Through particles prompt penetration electric fields (PPEFs) (which can be eastward or westward) depending on the interplanetary magnetic field IMF-Bz orientation, the energies are injected to the equatorial/low-latitude. However, disturbance dynamo electric fields (DDEFs) comes several hours after the storm commence, cause by Joule heating due to precipitation of charged particle in the polar region and is usually

experienced during the recovery phase. These electric field mechanisms (i.e. PPEF and DDEF) help in the redistribution of the plasma in the ionosphere (Amory-Mazaudier *et al.*, 2017). Geomagnetic storm effect on the ionosphere is known to cause ionospheric behaviour to deviate from their quiet time behaviour. The changes are due to the convection dynamo of charged particles from the magnetosphere to the ionosphere, thereby causing the excitation of neutral atoms in the ionosphere. The ionization absorbs radio waves in the high-frequency ranges, resulting in communication problems (radio wave propagation blocks out) and navigation position errors (Prölss, 1995; Mendillo, 2006; Malandraki and Crosby, 2018).

Several works have been done on the quiet time morphology/structure of the equatorial ionization anomaly (EIA), and its day-to-day variability has been associated with the daily variation in the vertical plasma drift (i.e. E × B drift) (e.g., Balan and Bailey, 1995; Bagiya *et al.*, 2009; Liu et al., 2011; Bolaji et al., 2017; Mo et al., 2017). The daily variation dynamo is a combination of the solar quiet variation and the zonal winds at low/equatorial-latitude. The equatorial electrojet (EEJ) as a proxy for quiet-time vertical E × B drift (driven by zonal electric fields generated by an ionospheric dynamo) controls the strength and latitudinal extent of the EIA, which is a function of ionization density concentration. Followed the variation of the local solar ionizing radiation, the E × B drift increases at the sunrise period, attaining the maximum strength at noontime and reduce during the nighttime periods (Adebesin et al., 2013b; Balan and Bailey 1995). This diurnal variation of F region E×B drift generates the plasma fountain and the anomaly structure in the low latitude region. Moreover, the eastward electric field and the geometry of the magnetic field in the region result in the upward E×B drift, uplifts magnetized plasma of the ionosphere to the region of lower recombination rates. As a result of the increased pressure gradient and gravity, the uplifted plasma diffuses downward along the magnetic field lines, hence, the plasma fountain effect (Fejer, 1981; Balan and Bailey 1995; Bagiya et al., 2009; Fejer, 2011). The synergy between these aforementioned field mechanisms and the ionization process gives the daily morphology of the EIA structure, which is characterized by a double hump (i.e. the crests) at either side of the equator and depression in the ionization density at the magnetic equator. At sunrise periods the ionization is weak, the electric field that drives vertical E×B drift is as well weak eastwardly, thereby producing a weak structure of EIA around the period (Fejer 1981; Dabas *et al.*, 1984; Balan and Bailey 1995). In the daytime, due to the E layer dynamo, the upward E×B drift causes the development of the EIA that attaining the maximum intensity in the noontime hours. At nighttime, the forward fountain becomes a reverse fountain soon after the downward drift known as a prereversal enhancement in the vertical drift at sunset period. That is, the sunrise period EIA structure is not too different from that of the nighttime (Adebesin et al., 2013b), except for the sunset period where the zonal electric field appears to be stronger eastwardly and uplift the plasma to the higher altitude region of lower recombination. Plasma uplift is symmetry to the magnetic equator and ionization convergence to the regions outside the fountain.

The quiet-time ionosphere described above can be modulated due to perturbation electric fields. The distribution of the ionospheric plasma depends on the penetrating electric fields originating from magnetospheric current dynamic mechanisms (Balan *et al.*, 2009a). That is, different direction of Electric field and IMF-Bz will create different magnetospheric and ionospheric PPEFs with different outcomes (Tsurutani et al., 2008). Therefore, southward/northward IMF- Bz and eastward/westward electric field will be considered as the expression for upward/downward vertical plasma drift. The disturbed time electric field during southward IMF-Bz modulated the ionospheric dynamo electric field and enhances the upward vertical plasma drift (E x B drift) (Kelly et al., 1979; 2003), thereby raises the equatorial and low-latitude ionospheric plasma to the region of lower recombination rate. At equatorial anomaly latitudes, the electrodynamics coupling is by two major fields convection processes, the PPEFs which are solar-wind-magnetospheric origin and the DDEFs which are storm-induced wind system that originates from the polar region (Le-Huy and Amory-Mazaudier, 2005; Wei *et al.*, 2015; Amory-Mazaudier *et al.*, 2017). During a geomagnetic storm, the EIA structures are modulated, reveals distinctive features due to the interplay of the convectional coupling of the solar wind - magnetospheric energy. Aside from the PPEF and DDEF, Abdu (2017) mentioned two other drivers that drive the vertical plasma drifts that produced the changes in ionospheric height at low latitude, that is, disturbance meridional winds and disturbance zonal winds which are important only near sunset. The combined effects of these convectional fields, thermospheric winds, and neutral composition changes are responsible for the hemispheric transport of ionized plasma that initiates equatorial ionization anomaly (Balan *et al.*, 2013; 2017; Astafyeva *et al.*, 2015). At the main and recovery phases of geomagnetic storms, the contribution of PPEFs and DDEFs with the background magnetic field mechanisms causes severe modification of electrodynamic processes at the equatorial and low-latitude ionosphere. Some of the consequences are, increase in TEC at the magnetic dip equator compared to the low-latitude (known as plasma fountain reversal), pronounce increase or positive storm at both hemispheres and significant reduce

plasma or negative storm at the dip equator (i.e. the strong signature of EIA) and weakening EIA (when the TEC enhancement is relatively reduced at the hemispheres).

Several studies had been carried out on the ionization transport effects during geomagnetic storms in the equatorial/low latitude region (Abdu, 1997; Tsurutani *et al.*, 2004; 2008; Horvath and Lovell, 2008; Fagundes *et al.*, 2016; Blagoveshchensky et al., 2018). These studies focus on the understanding the role of vertical coupling of the dynamo fields and other on the ionization anomaly process during a geomagnetic storm in the Earth's ionosphere. Tsurutani et al. (2004) and (2008) explained the complex role of PPEF and IMF-Bz associated with a positive and negative ionospheric storm at equatorial regions using TEC data. This report and several studies reported that plasma upward transport driven by PPEF and equatorward winds led to the positive ionospheric storm. Bagiya et al. (2017) studied the Indian sector and reported the dayside ionospheric disturbances during the main phase of the storm. They observed that the EIA strength increased as the magnitude of the storm increases, which was explained in terms of the storm-time varying electric fields. A study by Mansilla (2019), used ionosonde observatories, in the equatorial and low latitude ionosphere of the South American sector, and reported that EIA was modulated during the storm. They further reported that EIA strength was reduced at the main phase and increase at the recovery phase, the plasma transport structures which were explained in term PPEF, DDEF and neutral winds. Many researchers, used TEC observations, investigated the effects of St Patrick's storm of March 2015 on the equatorial ionization anomaly at different regions of the globe. Using satellite-based GPS-TEC data over African, American and Asian sectors, Astafyeva *et al.* (2015) and Nava *et al.* (2016) investigated the ionospheric response to March 17, 2015. The significant positive ionospheric storm at equatorial, low, and mid-latitude regions over the sectors and are related to the effective changes in the observed thermospheric wind circulation towards the equator due to the prevalence increase energy injection and joule heating. Amaechi *et al.* (2018) analysed the simultaneous TEC response time, similarities and differences in the anomaly occurrence over East and West Africa sector during the St. Patrick's Day storm of March 2015. They reported a significant TEC increase and decrease, resulting from PPEFs and DDEFs corresponding to the main and recovery phases of the storm and modified quiet time ionization at the equatorial anomaly latitudes. Tsurutani *et al.* (2008), Horvath and Lovell (2008) and Fagundes *et al.* (2016) used large scale GPS-TEC data from the non-African region to study the ionospheric response to some large geomagnetic storms. They reported a significant TEC enhancement at either side of the dip equator at the storm main phase. The strong EIA which arises from the simultaneous impulsive action of eastward PPEF and equatorward wind (Balan *et al.*, 2018).

Of all these effects, the modulated EIA structures have not been investigated in detail during geomagnetic storms in the Africa sector, most especially during the two recent identified St. Patrick's storms (i.e. March 2013 and March 2015). Studies have not ascertained the role of the southward interplanetary magnetic field (IMF-Bz) and Electric field (IEF) in driven of ionization anomaly structure in the equatorial/low-latitude region, especially during the two storms in the African region. It should be noted that for different storms we have different interplanetary structures controlling the current dynamo (Gonzalez *et al.*, 1999; Adekoya and Chukwuma, 2018). This may have discernible effects on the ionization structures at the anomaly regions produced by vertical plasma drifts driven by magnetospheric dynamo fields and the aforementioned wind systems. Tsurutani et al., (2008) has reported that northward orientation of IMF-Bz is expected to cause negative ionospheric storm during the daytime periods and intense southward turning of the IMF-Bz is associated with the dayside positive ionospheric storm. Therefore, we will look at the ionization effects in the equatorial and low-latitude in the narrow meridian of the Euro-African sector during the two St. Patrick's storms. And the role of the IMF-Bz and IEFy in the plasma transport structure of the EIA. The hourly changes of these interplanetary parameters structure and EIA structure will be investigated during the two storms. Further, the two storms were driven by sheath fields (the storm is due to the shock compression and draping) and the complex structure of solar plasma, that is, Sheath and Ejecta (Gonzalez *et al.*, 1999; Adekoya and Chukwuma, 2018), but with different magnitudes. The difference seems to depend on the rate of energy input (Adekoya and Chukwuma, 2018) from the magnetosphere during the storms in the ionosphere. For example, the Dst magnitude for March 17, 2013, is -131 nT and that of March 17, 2015, is -223 nT. This may cause a plasma fountain to exhibit a distinctive signature during the two storms. Also, based on the fact that the electrodynamic structure over Africa equatorial and low-latitude region ionosphere displays some distinctive features that are relatively different from those at other meridian sectors and crucial. Therefore, it will be of scientific advancement using experimental data from ground base GPS-TEC to investigate, aside from the qualitative classification of the EIA structure and reverse fountain effect signature, the implications of the changes in the magnitude of the storms over African equatorial anomaly latitudes region.

2. Data Acquisition and Methodology

The ground-based GPS receiver data used in this study were retrieved from African Geodetic Reference Frame (http://www.afrefdata.org) and International GNSS service (http://www.igs.org) during St. Patrick's Day storms of March 2013 and 2015. Figure 1 depicts the Euro-Africa map and the location of the GPS receivers/stations used in the investigation. The GPS receiver stations name, code, country, as well as their geographic and geomagnetic coordinates, were highlighted in Table 1. The geomagnetic index and solar wind parameters data used were obtained from the National Space Science centre's NSSDC OmniWeb Service (http://nssdc.gsfc.nasa.gov/omniweb). Further detail on the classification of the geomagnetic storm and interplanetary structure of the driver gases can be found in Adekoya and Chukwuma (2019).

The retrieved slant TEC (STEC) from the ground-based GPS data was corrected for satellite differential delay, receiver differential delay, and receiver inter-channel bias. The electron contents between a receiver on the ground and a satellite-based GPS at an altitude of ~20,200 km represent the STEC. The STEC was further processed by the geometric factor for estimation of absolute vertical total electron content (VTEC) for each GPS receiver (Mannucci et al., 1993; Hofmann-Wellenhof, 2001; Langley et al., 2002). The daily VTEC was estimated from all the visible satellites for every hour of the day, which was been refers to as TEC. More detail on the analysis of the ground-based GPS can be found in Bolaji et al. (2012) and (2013).

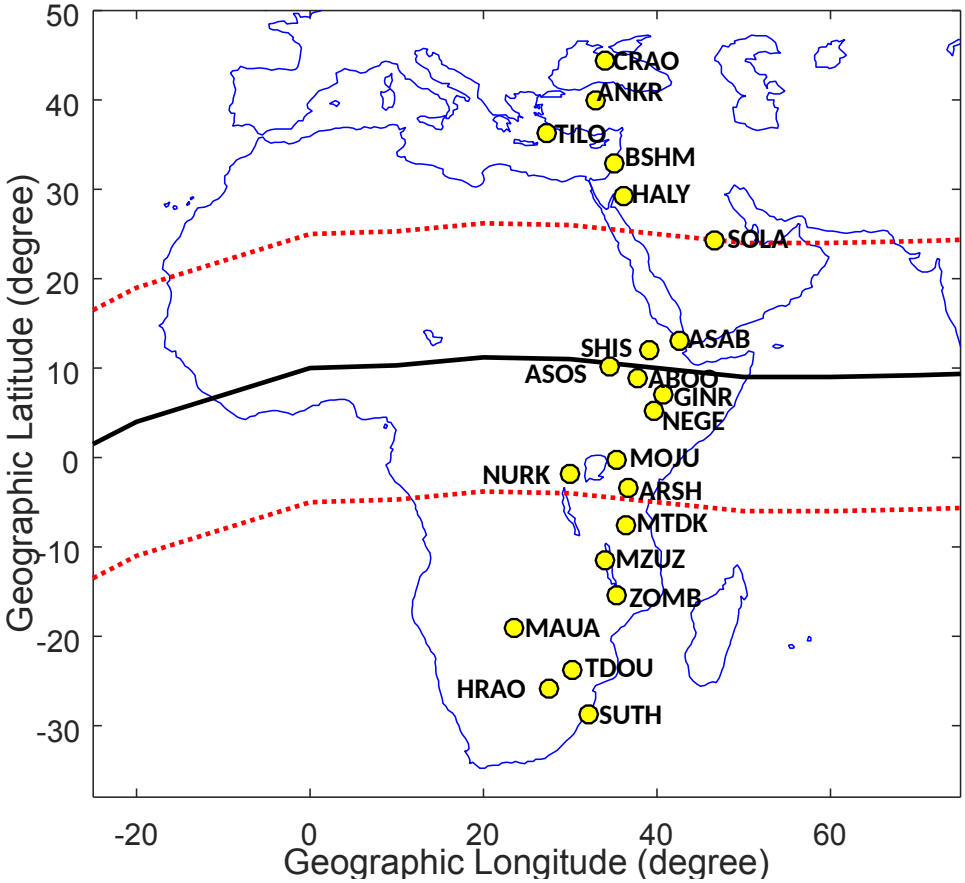

Fig. 1: The map showing the geographical location of the stations used.

Table 1: The detail list of the stations used and their geographic and geomagnetic coordinates

Station name/Country	Station Code	Geographic Coordinate	Geomagnetic Coordinate

Sutherland (South Africa)	SUTH	28.780S, 32.030E	38.570S, 102.820E
Hartebeesthoek (South Africa)	HRAO	25.89^{0}S, 27.68^{0}E	36.31^{0}S, 94.61^{0}E
Thohoyandou (South Africa)	TDOU	23.79^{0}S, 30.33^{0}E	34.10^{0}S, 98.37^{0}E
Ngamiland (Botswana)	MAUA	19.19^{0}S, 23.52^{0}E	30.12^{0}S, 92.51^{0}E
Zomba (Malawi)	ZOMB	15.37^{0}S, 35.32^{0}E	26.06^{0}S, 105.58^{0}E
Mzuzu (Malawi)	MZUZ	11.42^{0}S, 34.00^{0}E	21.87^{0}S, 104.91^{0}E
Mtandika (Malawi)	MTDK	7.54^{0}S, 36.42^{0}E	17.56^{0}S, 107.79^{0}E
Arusha (Tanzania)	ARSH	3.39^{0}S, 36.69^{0}E	13.03^{0}S, 10.32^{0}E
Kigali (Rwanda)	NURK	1.94^{0}S, 30.0^{0}E	11.62^{0}S, 101.57^{0}E
Eldoret (Kenya)	MOIU	0.28^{0}S, 35.29^{0}E	9.18^{0}S, 107.00^{0}E
Negele (Ethiopia)	NEGE	5.33^{0}N, 39.58^{0}E	3.60^{0}S, 111.33^{0}E
Ginir (Ethiopia)	GINR	7.14^{0}N, 40.70^{0}E	1.59^{0}S, 112.46^{0}E
Aboo (Ethiopia)	ABOO	8.99^{0}N, 37.80^{0}E	0.01^{0}N, 109.48^{0}E
Assosa (Ethiopia)	ASOS	10.05^{0}N, 34.55^{0}E	0.69^{0}N, 106.17^{0}E
Shimsheha (Ethiopia)	SHIS	12.00^{0}N, 38.98^{0}E	3.28^{0}N, 110.62^{0}E
Asab (Ethiopia)	ASAB	13.06^{0}N, 42.65^{0}E	6.79^{0}N, 110.47^{0}E
Solar Village (Saudi Arabia)	SOLA	24.26^{0}N, 46.51^{0}E	17.71^{0}N, 118.16^{0}E
Halat Ammar (Saudi Arabia)	HALY	29.16^{0}N, 36.07^{0}E	21.85^{0}N, 107.53^{0}E
705, Nesher (Israel)	BSHM	32.77^{0}N, 35.02^{0}E	26.00^{0}N, 106.62^{0}E
Karpathio Pelagos (Greece)	TILO	36.38^{0}N, 27.39^{0}E	29.45^{0}N, 99.46^{0}E
Altındağ/Ankara (Turkey)	ANKR	39.93^{0}N, 32.85^{0}E	34.29^{0}N, 105.06^{0}E
Crimean Peninsula	CRAO	44.41^{0}N, 33.99^{0}E	39.48^{0}N, 106.71^{0}E

3. Results

3.1 Interplanetary and magnetic structure of storm of March 16 – 18, 2013

Figure 2 presents the geomagnetic and interplanetary phenomena that drive the intense St Patrick's geomagnetic activity of 16 -17 March 2013, which is the second major geomagnetic storm of the ascending phase of solar cycle 24. The plots were presented for three days before and after the March 17 which is the day of the maximum activity of the storm (i.e., the storm main phase). This is for proper analysis of the event that preceded and exceeded the initial and recovery phases of the storm. Looking at figure 2a, one can see that on March 14 - 16 the geomagnetic activity was quiet with indication of disturbance storm time (Dst) plot showing a minimum peak response of -23 nT. The storm commences on March 17 around 0500UT with a sudden increase in the Dst plot corresponding to sharp increase in plasma speed (Fig. 2b) from 414 km at about 0500UT to 725 km at 1200 UT noontime. This subsequently increased the plasma temperature, the plasma pressure and the proton density to the peak values of 529522 K, 5.96 nPa and 8.5 N/cm^3 coincided with the sudden Dst increase of 15 nT at about 0600 UT. Immediately after its peak magnitude of 15 nT, its commenced downward excursion reached a minimum of -131 nT at about 2100UT the same day and gradually recovered throughout the remaining days. A close inspection of the storm parameters at the period of sudden commencement indicates that there was southward turning of the interplanetary magnetic field (IMF-Bz) and eastward electric field to the peak magnitude of 14.4 nT and 9.71 mV/m at about 0900UT on March 17. Both fields appear to fluctuate with an attempt to change their orientation, but reverses and maintain the same direction, with the second peak values of -11.5 nT and 7.13 mV/m around 1800 UT at the storm main phase. However, this behaviour was reversed as the storm progressively recovered. Also, observation showed that the ratio of magnetospheric plasma thermal pressure to the magnetic pressure, that is, plasma beta of magnetosheath flow around this period was 2.28 at about 0700UT and 2.61 at about 1400UT corresponding to the Bz southward turning and the main phase period. Similarly, the peak value of proton density of 1.03 N/cm^3 was recorded at about 0800UT, at the descending phase of the Dst before it decreases throughout the recovery phase. The same fit of high variation was observed for plasma temperature and the plasma pressure with peak values of 522960 K and 12.45 nPa at about 0700 and 0800 UT respectively. The characteristic of the solar wind phenomena of this storm indicates that the storm was due to the shock

compression and draping, and the complex structure of solar plasma, known as sheath field and ejecta, the CME-Driven storm characteristic explained in Adekoya and Chukwuma (2018).

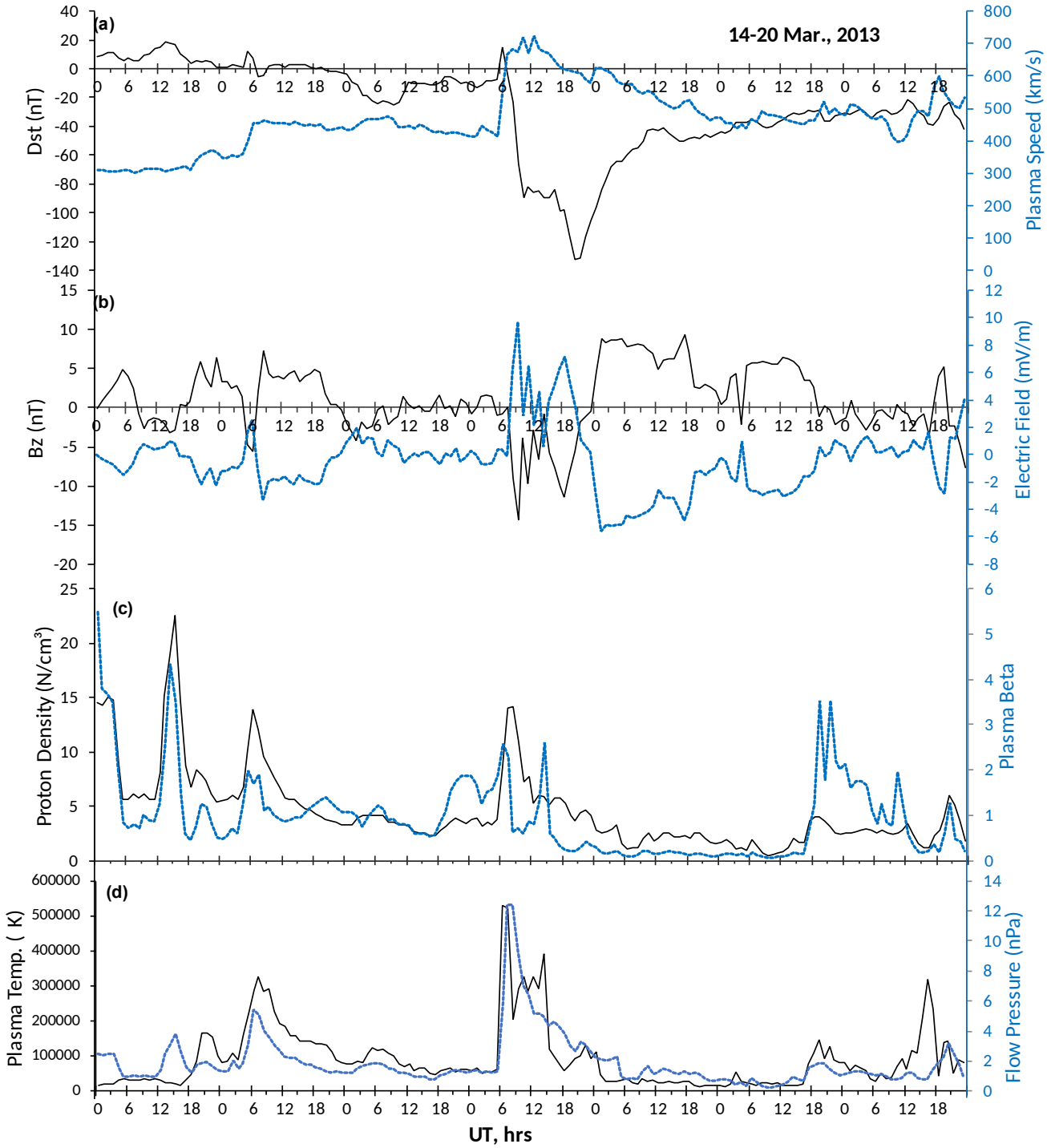

Fig. 2: Geomagnetic and interplanetary structure of the storm of March 2013. The period spans the March 14 – 20, which covers the initial, main and the recovery phases of the storm.

3.2 Ionospheric GPS-TEC response to the storm of March 16 – 19, 2013

To investigate the ionospheric anomaly behaviour at the equatorial and low latitude ionosphere to the intense geomagnetic storm of March 2013, the temporal changes of GPS-TEC at a narrow Africa meridian within the geomagnetic latitude ranges between 40° and 45° in the northern and southern hemisphere were studied. The hourly GPS-TEC response to the storm across the latitudes which covers the initial, main and recovery phases of the storm was presented in Figure 3. The GPS-TEC variations for each hour of the day were plotted against universal time (local time). This allows the detailed study of the ionization anomaly processes and explicable in

terms of the electrodynamical processes, that is, its relationship with vertical E × B drift in response to the geomagnetic disturbances. It should be noted that the storm began its campaign with shock at about 0500 UT on March 17. For convenience, March 15 – 16 are referred to as initial phase and the days exceeding the storm day (i.e. March 17) are referred to as recovery phase.

Figure 3a presents the TEC variation for the first four hours of the day (i.e. 0000 – 0300 UT/ 0220 – 0520 LT) of the storm and the respective initial and recovery days. The TEC exhibits double humps, one hump in each hemisphere, which majorly formed between 15° – 20° latitude with a decrease at the magnetic equator. Around these periods the TEC variation was less than 10 TECU for all days under consideration except on March 18 – 20 around 0000 UT that the TEC recorded peak values of ~ 20 TECU in the northern hemisphere. Around these periods, there is a northward orientation of IMF-Bz and the electric field was westward (Fig. 2). That is, the upward drift was inhibited due to the increase the plasma recombination processes. Therefore, the observed weak equatorial ionization anomaly (EIA) may be related to the quiet geomagnetic/nighttime plasma drift condition during the initial phase, but that of the recovery phase may be due to the pre-conditioning processes (nighttime process) of the disturbance dynamo.

Figure 3b shows that TEC magnitude increases with the time of the day. The TEC variation which recorded an increase at the equator reached ~30 – 40 TECU around 0500 – 0700 UT (0720 – 0920 LT) and decreased at the hemispheres, hence the equatorial peak. This time frame was in the sunrise period, and the strength of the vertical E × B drift is weak and no magnetospheric convection was recorded as observed from Fig. 2b. The TEC variation around these periods exhibited a reversed EIA structure. The structure which may due to the downward motion of the plasma drift when the zonal electric field is westward (Balan et al., 2009a). In Fig. 2b, the E- field intensity was reduced and westward and the IMF-Bz was also reduced and northward. The orientation, which suggests downward drift motion of the plasma due to lower particle penetration. Also, one should note that these periods on March 17 coincided with the SSC. The peaks of E-field and IMF-Bz recorded around these periods were -0.07 mV/m and 0.1 nT respectively. Therefore, the equatorial TEC enhancement/equatorial peak may likely be related to the soft particle precipitation or sudden magnetospheric electric field penetration (Adekoya and Adebesin, 2015; Danilov, 2013; Adekoya et al., 2012b).

Observing fig. 3c, the equatorial peak persisted and become more pronounced around 0800 – 0900 UT as the TEC recorded on average 60 TECU. Thereafter, around 1000-1100, pre-noon hours, the increased TEC has started shifting from the dip equator toward the higher latitude region and, rather, formed TEC crest at both hemispheres. From 1000 – 1100 UT (1220 – 1320 LT) one can see that the plasma gradually bifurcated into two crests formed at the hemispheres. The driving mechanisms can be explained from the superposed interplanetary fields plot of Fig. 2b, because the northward Bz and westward electric field variations are more conspicuous. However, on March 17, due to the gradual convection of magnetospheric energy, the electric field was seen to have changed its orientation eastwardly and IMF-Bz southwardly, and are intense. This perturbed field modified the vertical drift around these periods and produced the changes in the observed TEC variation. Owing to the modified E × B drift caused by the enhanced eastward electric field, the plasma fountain strengthened. Plasma bifurcation into two crests was symmetry with the fountain effect at the periods, hence the equatorial ionization anomaly. Further observation showed that the formed TEC enhancement in the northern sector is larger than it appears in the southern sector. Also, looking at the TEC magnitude (i.e. ~50 – 65 TECU), it was obvious that ionization has increased around these periods too.

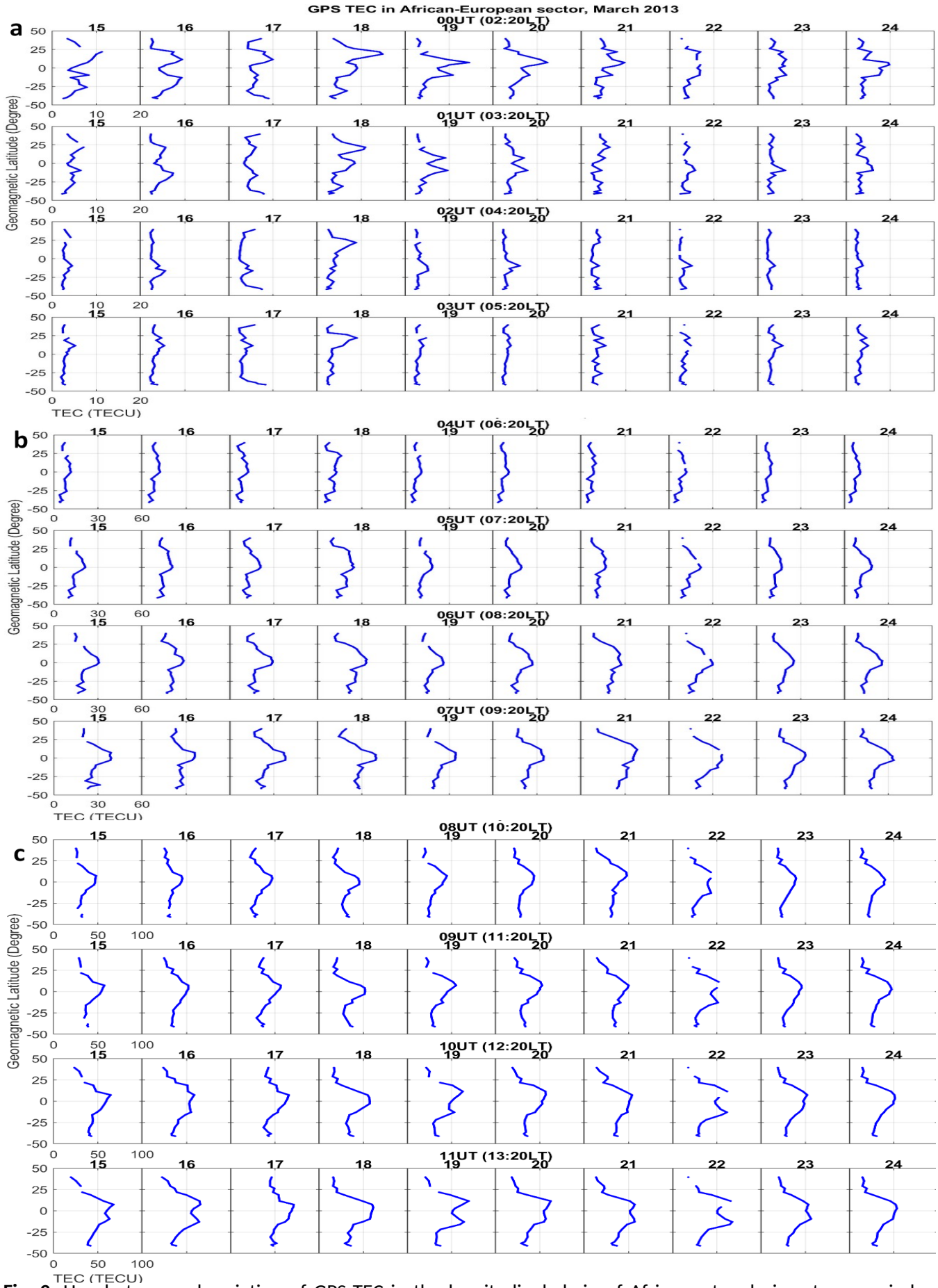

Fig. 3: Hourly temporal variation of GPS-TEC in the longitudinal chain of Africa sector during storm periods of March 15 – 24, 2013.

In Figure 3d, the ionization anomaly becomes more conspicuous, the TEC enhancements at higher latitudes and a decrease at the dip equator are now stronger during the initial and recovery phases. However, on March 17, a weak EIA structure was observed. At 1200UT, the TEC bifurcation was weak, the corresponding drivers, electric field and Bz recorded peak values of 2.1 mV/m and -2.9 nT (see Fig. 2b). Similarly, at 1300 UT (1520 LT) the field strength mechanisms were weak and the observed TEC variation depicts a rather suppressed EIA structure, as the TEC appears to be only accrued in the northern hemisphere. As time progresses the E x B drift gradually regain its strength, thereby produced a more noticeable but weak EIA structure at 1500 UT (1720 LT). The electric field flow and Bz orientation at this period recorded peak values 3.89 mV/m and -5.8 nT (Fig. 2b). Looking at the TEC variation at 1500 UT (1720 LT) onward, the TEC formed hemispheric crest was generally higher in the southern hemisphere, making the ionization concentration to be larger in the southern hemisphere than it appears in the northern hemisphere. That is, the thermospheric circulation and meridional wind were more induced during the storm at the southern hemisphere, hence the TEC enhancement at the hemisphere.

Similarly, around 1600 – 1900 UT the ionization anomaly persisted and stronger (Figure 3e). Around these periods the vertical drift increases, as can be seen from the intense nature of the eastward electric field and southward Bz (Fig. 2b), hence the forward plasma fountain effect. The TEC increase at either side of the dip equator and a decrease at the dip equator was significant. The TEC peak was on the average > 50 TECU in the southern hemisphere and ≤ 50 TECU in the northern hemisphere. The TEC decrease at the dip equator was 20 TECU on the average. The crest-to-trough ratio of TEC in the northern hemisphere (≤ 2.5) was lower compared to the southern hemisphere (>2.5). This also indicates that the increase in the crest-to-trough ratio signifies the anomaly strength and significance due to PPEF and the presence of storm time equatorward wind (Tsurutani *et al*., 2008; Balan *et al*., 2009a). Around 2000 – 2300 UT (Figure 3f) the TEC variation did not show any contrary behaviour, only that the anomaly strength appears to be more suppressed than at the sunset period. At these periods, the maximum magnitude of the Dst was -132 nT, the TEC magnitude has decreased drastically because the vertical drift was downward as indicative in Fig. 2b.

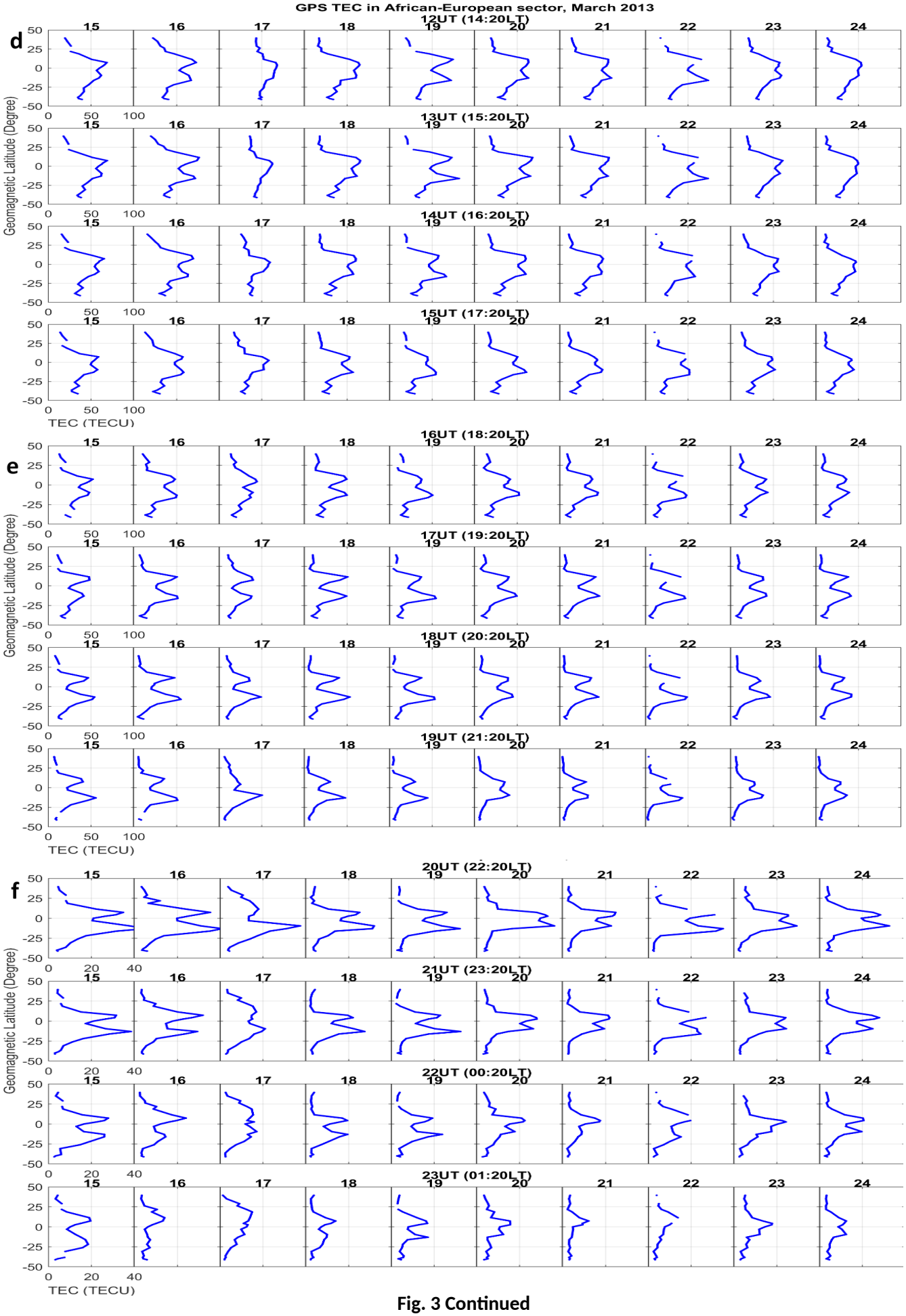

Fig. 3 Continued

3.3 Interplanetary and Magnetic structure of March 16 – 18, 2015 geomagnetic storm

Figure 4 presents the circumstances of the solar wind parameters associated with the geomagnetic storm of March 16 – 18 2015, the St Patrick's day storm, the most intense storm of solar cycle 24. The geomagnetic storm initialised its evolution on March 17 with a sudden increase in Dst around 0300 – 0800 UT to peak response of 56 nT at about 0500 UT (Fig. 4a), and was preceded by a relatively quiet geomagnetic condition. It was observed from the SSC period that the plasma speed was suddenly increased exponentially from 410 km at 0400 UT to 597 km at 1500UT of the main phase. Thereafter, the intensity of the storm gradually increases as the Dst decreased to the minimum peak magnitude of -223 nT at about 2200UT on March 17. During the SSC periods, the IMF-Bz orientate southward to the peak of -16.3 nT at about 0800UT. Sharply it turned northward and immediately changed polarity back to the southward where it attained its maximum magnitude of 18.1 nT at about 1500 UT. In the reversed order to the IMF-Bz, the electric field attained peak magnitudes of 9.13 and 10.45 mV/m at 0800 and 1500 UT corresponds to the SSC and main phase periods (Figure 4b). Although the amplitude of the eastward electric field was low compared to the threshold value of 13 mV/m reported for strong/great storms by Adekoya and Chukwuma (2018), it was transpired from the intense southward magnetic field with long duration of orientation and strong westward ring current energy that the storm may be categorised as a very intense/great storm. The Plasma beta and Proton density plot did not show any contrary morphology compared to what was observed during the St Patrick's storm of March 2013. The peak value corresponding to the SSC period was 2.44 and 38.5 Ncm^3, which decreases through the main and the recovery phases (Figure 4c). The plasma temperature and flow pressure responded to the shocked and compressed fields with an increase that maximized at about 1100 and 1600 UT with peak magnitudes 912227 K and 20.76 nPa respectively, at the main phase.

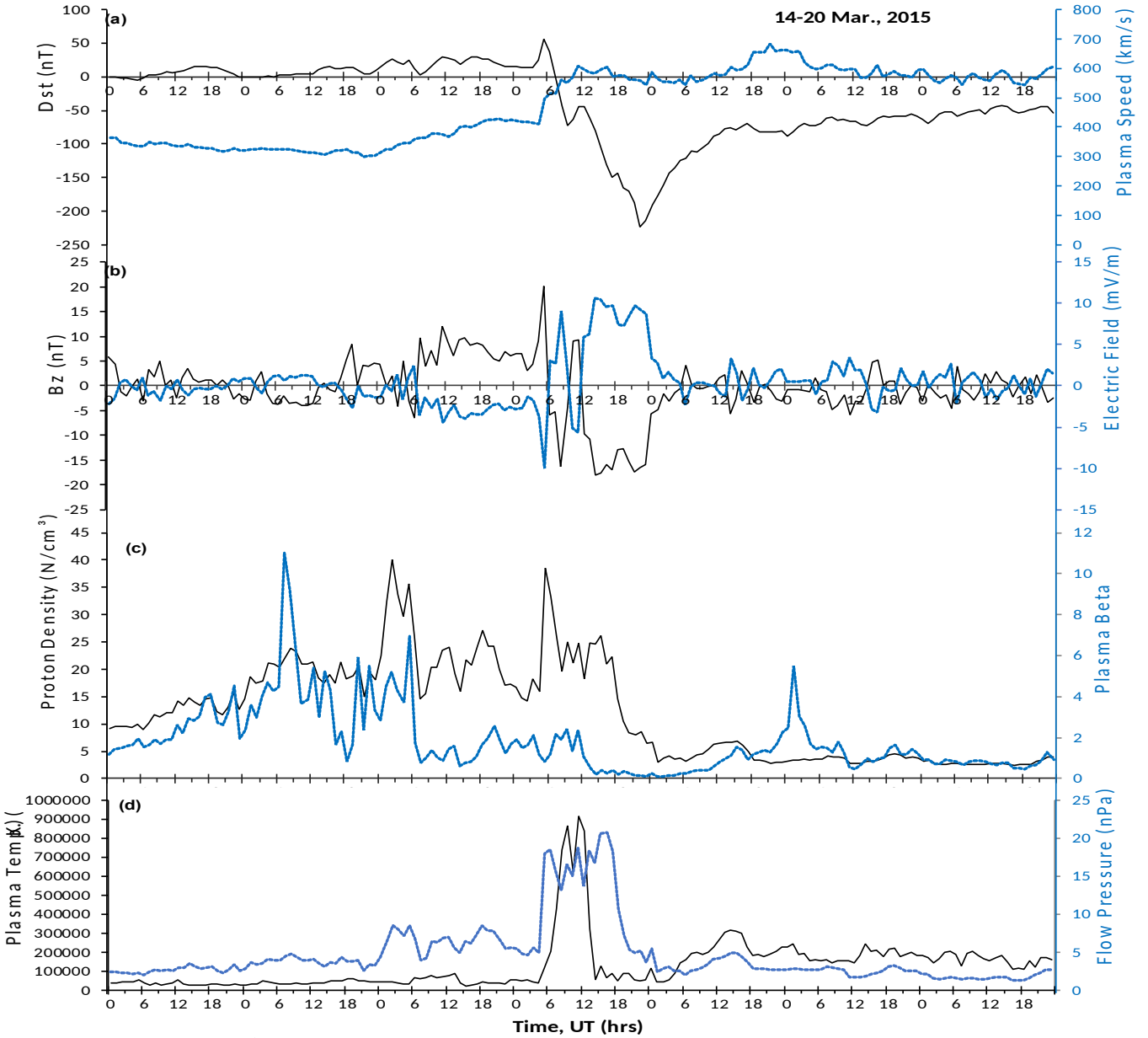

Fig. 4: Same as Fig. 2, but for St Patrick's day storm of March 2015.

3.4 Overview of the GPS-TEC behaviour to the storm of March 16 – 19, 2015

Figure 5 (a – f) presents the TEC variation during the St Patrick's storm of March 2015 at equatorial anomaly region and beyond in a meridian of the Africa sector. The hourly TEC variation was presented for two days before the storm (initial phase), the day of the storm (main phase) and the recovery days respectively. The TEC observation shows a distinctive characteristic regarding the time of the day and the phases of the storm. Presented are the observed characteristics of the TEC variation as it explained the electrodynamics of plasma and ionization anomaly during the period of the storm.

Figure 5a shows the TEC variation for the first four hours of the considered storm periods. It was revealed that TEC variation around these periods was low, the peak magnitude here was < 15 TECU, indicating no significant changes in the TEC, and variations that are similar to nighttime conditions. Also, the TEC variations exhibited an inconsistent behaviour on March 15 – 16, the TEC shows an enhancement in the southern hemisphere and a rather smooth variation in the northern hemisphere. The orientations of the IMF-Bz and electric field flow around these periods indicated downward E × B drift (fig. 4b). Owing to the downward drift, the thermospheric (or neutral) winds controlled the plasma transport, blow the ionospheric plasma across the magnetic field from the northern to the southern (Rishbeth 1998; Adekoya and Adebesin, 2014; Namgaladze et al., 2000; Adebesin et al., 2019), hence the hemispheric asymmetry of the TEC. Similarly, it was observed on March 17 that the northern plasma enhancement was outside the anomaly region. Nevertheless, the TEC variation indicates crest on either side of the dip equator and a trough at the dip equator sequel to the quiet time geomagnetic condition at the periods. The recovery phase TEC variation did not show contrary behaviour compared to March 15 – 17. However, the EIA structure was rather perceptible around 0300 UT (0520 LT), the pre-sunrise period.

The sunrise time TEC variation in figure 5b shows the synergy between the geomagnetic storm and the ionospheric plasma around 0400 – 0700 UT (0620 – 0920 UT). Followed the pre-sunrise weak EIA structure, the TEC variation at sunrise periods was more enhanced and, the EIA structure, though was weak, but was more significant. The TEC increases from the initial magnitude < 20 TECU at about 0400 UT to TEC > 55 TECU around 0700 UT. Around these periods for all the days under consideration, it was observed that the E x B drift was upward, but very weak as the Bz orientated southward with peak values ranges 1 - 3.5 nT and electric field moved eastward attained peak values ranges 1.13 – 3.38 mV/m, except for March 17 (see Fig. 4b). On March 17, these periods happened to be the SSC period, the TEC responded to this with a low TEC variation compared to the other phases of the storm. A weak EIA structure/plasma fountain effect was observed with a slight increase in TEC in the northern hemisphere than the southern hemisphere, owing to the sudden significant reversed E×B drift (see fig. 4b). The electric field and IMF-Bz variations indicate plasma drift reversal or downward drift. A similar observation of TEC behaviour was observed in the recovery phase but the magnitude of the TEC variation was distinct and more increased at these periods.

Figure 5c presents the local pre-noontime – noontime storm-time TEC variation around 1020 – 1320 LT (0800 – 1100 UT). There was rapid storm-time energy penetration combined with the daytime ionization processes that increased and strengthened the TEC variation. This is evident in Figure 5c, as the TEC magnitude increased to ~75 TECU around 1100 UT sequel of prompt penetration at the main phase. On March 17, the TEC bifurcation was more protuberance at the hemispheres making the EIA structure to be perceptible compared to the other days. As observed in Fig. 4b, the E-field was eastward and Bz was southward with peak values of 9.13 mV/m and 16.3 nT at about 0800 UT indicating strong prompt equatorward penetration, forming plasma fountain effect. Thereafter, around 0900 – 1100 UT the E x B drift reverses, the EIA structure becomes more apparent than when E x B drift upward (i.e. prompt penetration electric field). On March 15 – 16, it was observed that the TEC enhancement located away from the equator was also displaced to higher latitudes. These days were considered geomagnetic quiet times, the EIA structure was more apparent at noontime (1120 – 1320 LT) than pre-noontime (1020 – 1120 LT). The EIA formed as a result of the quiet time electrodynamics forces (i.e. E x B forces, gravitational forces photoionization) and recombination (Tsurutani *et al*., 2008) which leads to TEC enhancement at off equator. Further on March 18 – 19, the reduced pressure suggests low particle penetration, and the reduced E-field intensity (the electric field was eastward, but very weak) suggests reduced prompt penetration of E-field (Fig. 4b). Therefore, the plasma transport was due to the disturbance dynamo driven by the global thermospheric circulation resulting from the energy input at the high latitude and disturbance winds (Abdu, 1997).

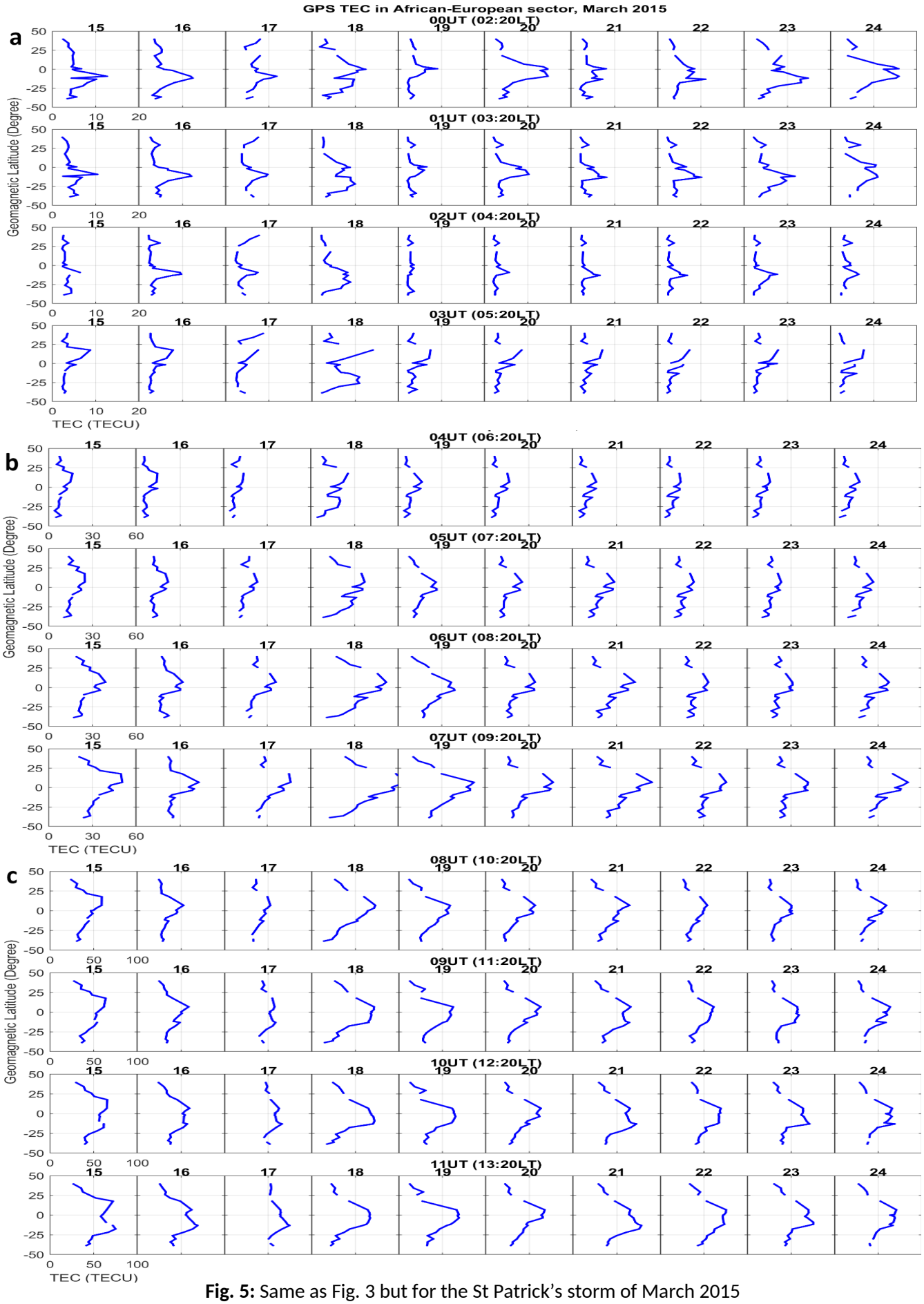

Fig. 5: Same as Fig. 3 but for the St Patrick's storm of March 2015

The daytime (post-noontime) TEC variation around 1200 – 1500 UT (1420 – 1720 LT) was presented in Figure 5d. These periods at the initial phase explain the TEC response to the quiet time electrodynamic process. At the storm main phase (i.e., March 17), it elucidates the continuous precipitation of geomagnetic energy as it affects the electrodynamic processes of ionospheric plasma and neutral wind. While the recovery phase explains the aftermath effect of the deposited energy as it induced the thermospheric circulation and westward electric field through disturbance dynamo processes in the ionosphere in the region. Observing the TEC variation during the initial phase of the storm, equatorial depletion and hemispheric enhancement were more noticed. The role of quiet time electromagnetic forces and recombination becomes more apparent, the quiet-time plasma fountain effect. Also, one can identify the asymmetry in the NH and SH, the TEC enhancement is stronger in the SH than in the NH, which may find their explanation in the meridional wind circulation aided by the cross equatorward wind system across the hemispheres. On the other hand, one can see the suppression in the ionization anomaly on March 17 around 1200 UT due to the strong E × B drift (i.e. increased eastward E-field). As the strength of the storm-time dynamo increased, hemispheric TEC enhancement was seen to gradually converging near the equator. Similar TEC behaviour has been observed during the storm of March 2013 which was limited to the post-noontime periods due to the reduced strength of the storm-time dynamo forces and current mechanisms at the periods. However, the spectacular observation in TEC variation due to the increased storm dynamic strength and magnitude shall be explained in the next paragraph. During the recovery phase, especially on March 18 - 20 around 1200 – 1300 UT, though the TEC variation magnitudes were stronger (TEC ≈ 70 TECU), the hemispheric TEC enhancement was displaced near the equator. On this day, there was no prompt penetration, the disturbance dynamo circulation processes such as DDEF, equatorward neutral wind (increase in poleward plasma wind flow that lower the ionosphere to the altitudes of increase chemical loss) and westward zonal electric field controlled the plasma drift. The weak plasma fountain effect was thereafter exhibited by TEC variation and maintained throughout the remaining days.

The TEC variation in Figure 5e exhibited the same behaviour as observed in Figure 5d throughout the days preceded and exceeded the storm day. There TEC variation at the equatorial region was greatly depleted and registered strong enhancement at the higher latitudes. On March 17, following the near-equatorial hemispheric TEC enhancements around 1600 – 1700 UT, the TEC recorded a spectacular and distinctive variation at 1800 – 1900 UT (2020 – 2120 LT). There was a convergence of the hemispheric enhancements at the equator, that is, the TEC exhibited a reversed EIA structure, known as equatorial peak or reversed plasma fountain effect. This reversed EIA structure can be justified from the intense eastward E-field and southward Bz around these periods. Further, these periods of the observed equatorial peaks were at the sunset PRE periods, the TEC variation is expected to decrease at the equator as the plasma transport is controlled by the dynamo effects at low latitude. However, the plasma transport was driven by PPEF originating from the magnetospheric current dynamics mechanisms and equatorward winds that led to the positive ionospheric storm. This observed positive storm at the equator extended till around 2000 UT (2220 LT) (Fig. 5f). The TEC magnitude, though was lower, exhibited a discernible equatorial peak. Thereafter, the TEC variation experienced bifurcation into two hemispheric crests near the equator, gradually, as the storm recovered the TEC magnitude reduced and the EIA effect becomes obvious. Likewise, on March 18 the TEC variations depict an equatorial peak characteristic, the nighttime TEC enhancement magnitude decreases as the with increased in time. Further observation of Fig. 4b revealed that the plasma transport was due to disturbance dynamo as the storm recovered, eastward E-filed and southward Bz strengths/magnitudes was low and remain insignificant. In essence, the disturbance dynamo electric field produced by the thermospheric storm time circulation and neutral winds (poleward plasma flux) through joule heating originated from the deposited energy (Astafyeva *et al.*, 2015; Nava *et al.*, 2016).

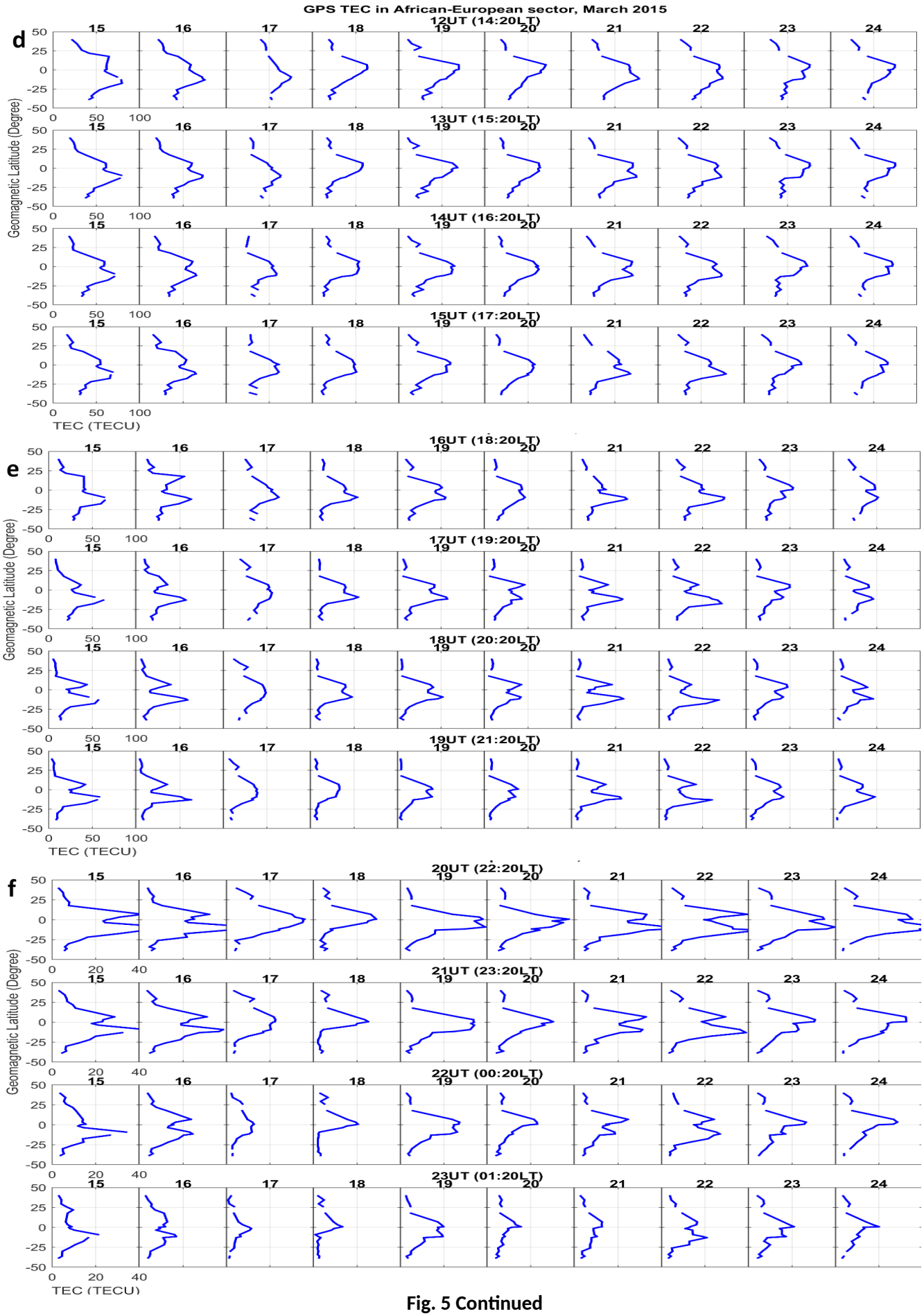

Fig. 5 Continued

4. Discussion and Conclusions

Geomagnetic storm/sub-storm is more protuberant in causing larger particle precipitation and an increase in the strength of the electric field (Kelly et al., 1979), which make the plasma disturbances to be stronger and variable in the ionosphere. During the two geomagnetic storms, we took into account the driver gases of the storms according to the intense southward IMF-Bz strength (Gonzalez et al., 2001; Echer et al., 2008; Wang et al., 2010; Adekoya and Chukwuma 2018). Not only that, we also considered other solar wind parameters accompanied the IMF-Bz, that is, the plasma flow speed, plasma pressure, plasma beta and plasma temperature, which were viable parameters used in classifying the main driver gas of storms (see Adekoya et al., 2012a; 2012b; Adekoya and Adebesin 2015). From the observed characteristics of the solar wind parameters associated with the southward Bz, the storms were driven by sheath field and complex ejecta. The driver gas resulted from the compression and draping and the complex structure of solar wind plasma, the CME characteristic (Adekoya and Chukwuma, 2018). However, the same plasma structures produced different magnitudes of energy, hence different storm magnitudes. Adekoya and Chukwuma (2018) reported that the magnitude of an intense geomagnetic storm is determined by the intense nature of the electric field strength. The higher storm magnitude of March 2015 was associated with the long-duration of high eastward electric fields strength and intense southward IMF-Bz compared to that of March 2013. The decrease/increase in plasma pressure suggests the decrease/increase in particle penetration. It was further observed that different course of electric field and IMF-Bz create different magnetospheric and ionospheric penetration electric fields. However, not all great storms produce intense ionospheric storm (Balan et al., 2013), because some large amounts of magnetospheric energy are input in a short duration and decay faster than when long-lived energy is produced. That is, the strong storm was driven by the large eastward electric field caused by long-duration penetration electric fields (Gonzalez *et al*., 2001; Wang *et al*., 2010) that produce severe ionospheric storm, thus, the distinctive equatorial ionization anomaly structure.

Generally, the observed TEC variations revealed ionospheric positive storm at the hemispheres and negative storm at the equator, the variation which is known as the effect of plasma fountain or EIA. Sometimes, the TEC variations during the daytime reversed, the higher latitudes (hemispheric) crest become suppressed and equatorial TEC decrease turned positive. This anomaly structure was especially observed at the main phase of the storms of March 2015, and at the initial and recovery phases of the two storms. The reversed EIA structure at the equator arises under the intense action of eastward prompt penetration electric field during intense southward IMF-Bz and equatorward wind. The daytime reversal at the recovery and the initial phase (SSC period) was understood to be the consequence of the westward electric field and the meridional component of neutral wind (poleward wind), optimized by the disturbance dynamo fields, hence, the equatorial peak. The variations of IMF-Bz and the E-field, which possibly interpreted in terms of the E × B drift, drive the TEC variation. The enhanced E-field intensity, which probably meant enhanced E x B drift effect.

Our results showed that TEC variations are consistent with the interplanetary conditions during the phases of the storms. The hourly EIA structures as recorded by TEC variation changes based on the hourly directions of E-field and associated IMF-Bz. The southward/northward and eastward/westward IMF-Bz and E-field instigates ionospheric dynamo electric field and vertical plasma drift that drives the ionospheric plasma that controls the development of equatorial ionization anomaly (Fejer, 1997; Adebesin et al., 2019). The contribution of plasma diffusion might be important, but not sufficient to account for the equatorial ionization anomaly (Rishbeth et al., 1963). Our observations revealed that the TEC variation was more accrued during the recovery and initial phases that the main phase of the storms. Even, the hemispheric TEC enhancements were higher and more variable than it appears during the PPEFs period. According to Balan et al. (2013), the eastward PPEF would optimize the plasma drifting and strengthen the EIA, in the presence of strong equatorward wind to produce more significant plasma fountain effect. That is, PPEF can produce forward plasma fountain, sometimes, plasma reversal depending on the nature of the wind and equatorial zonal electric field, but cannot strengthen it (Vijaya Lekshmi et al., 2007). On this note, the plasma fountain effect/EIA structure (positive ionospheric storm at the hemispheres), which was prominently observed around 1600 – 1900 UT (1820 – 2120 LT) on March 17, 2013, could be due to the enhanced eastward electric field (see Fig. 3) and equatorward neutral wind. Because the E-field was seen to be enhanced and eastward around these periods (see Fig. 2b), and probably increased the upward E × B drift effect. However, plasma reversal was seen around these periods as displayed by TEC variations during the storm of March 2015 (Fig. 5e). The reversal build-up from 1600 UT as the hemispheric TEC enhancements converged near the equator, around 2020 – 2120 LT the equatorial peak becomes apparent and significant. The interplanetary structures showed that the E × B drift was greatly intensified and eastward as it was

driven by PPEF (Fig. 4b). The PPEF originated from the dynamo mechanisms of the magnetospheric current and equatorward winds led to the positive storm (Balan et al., 2009b). Therefore, the driven phenomena for this observed reversed EIA structure (plasma reversal/equatorial peak) could be relatives to the high intensity of the electrodynamics mechanisms and strong equatorward neutral winds which could impose westward zonal electric field. Also, the reversed plasma fountain pointed to the fact that PPEF alone is unlikely to induce EIA, but with the presence of zonal electric fields imposed by the equatorward wind.

It is a well-established fact that the equatorial zonal electric field (eastward and westward) plays a prominent role in the plasma distribution at the equatorial and low latitude ionosphere under geomagnetic quiet and disturbed conditions (Balan et al., 2009a; 2013; 2018). That is, during a geomagnetic storm, strong equatorward winds through westward zonal electric field could inhibit plasma fountain or activate reversed plasma fountain effect that imposed the equatorial TEC enhancement. However, aside from the disturbance dynamo fields arising from the joule heating, the optimization of the thermospheric circulation, neutral wind, equatorial zonal electric field and the downwelling effect of wind could be the possible mechanisms causing the plasma reversal at the recovery phases (Balan et al., 2013, 2017). This reversed EIA structure, as it has a relationship with the interplanetary structure of the intensity geomagnetic storm may as also differ across sectors. This is due to the fact that the several works on equatorial and low-latitude ionosphere response during the St. Patrick's storm of March 2015, in other sectors of the globe have not in any way mentioned or reported this discernible TEC observation (e.g. Nava et al., 2016; Tulasi Ram et al., 2016, Fagundes et al., 2016, Astefyeva et al., 2015, Horvath and Lovell, 2008). This further affirmed the peculiarity in ionization instabilities in the African sector (Yizengaw et al., 2013) due to its geomagnetic properties and electrodynamics complexities compared to other sectors that have been reported. Hence, the curiosity in the study of the occurrence and characteristics of an equatorial ionospheric anomaly in the Africa sector.

The foregoing storm-time electrodynamic mechanisms and their influence on the ionosphere during the two storms was further elucidated using figure 6 (a and b). Figure 6a presents the daily overview of the TEC variation and delineates the daily structural behaviour of equatorial ionization anomaly (EIA) in the Africa sector in response to the storm of March 2013. Looking at the figure, one can see that the TEC variation was higher at the higher latitudes than it appears at the equator on March 15 and 16, indicating the effect of plasma fountain. Around these periods, there was no storm-induced energy, the Dst values for these days were invariably low, the E-field and IMF-Bz were mostly reversed and insignificant, hence the plasma fountain effect which was weak in the morning and nighttime periods. The quiet-time processes which include photoionization, thermospheric/neutral composition, zonal electric field (westward at dusk-dawn and eastward at dawn-dusk) and meridional wind (Balan et al., 2009a; Balan et al., 2013). Tsurutani et al. (2008) reported that photoionization will restore plasma densities at lower altitudes, leading to substantial increases in the TEC of the height integrated ionospheric electrons. During the daytime when the electrons become ionized, the eastward zonal electric field causes the upward vertical drift that uplifts the plasma to higher altitudes. Also noted was that during these days the TEC enhancement was higher in the northern hemisphere than it appears in the southern hemisphere. The hemispheric asymmetry may be induced by the presence of quiet-time cross-equatorial wind. The meridional wind intensifies the TEC enhancement at the northern hemisphere, and the increase poleward wind may be responsible for the lesser TEC variation in the southern hemisphere (see Balan et al., 2009a). However, on March 17 the hourly behaviour shows TEC enhancement at the equator around the sunrise period (0600 – 0920 LT) with increasing TEC values ranges 25 – 50 TECU, indicating an equatorial peak. These periods coincided with the sudden storm commencement (SSC) when the convectional fields (IEF and IMF-Bz) are reversed and insignificant.

Considering the TEC behaviour at the SSC period during the two storms, it was observed that SSC-TEC variation of March 2013 exhibited equatorial peak behaviour compare to the weak plasma fountain that was depicted during March 2015 (see Fig. 3 and 5). On March 2015, the electric field was westward with a peak value of 9.97 mV/m and the IMF-Bz was northward with a peak value of 20.1 nT around 0500 UT compared to approximately zero values recorded on March 2013. This posit that ionospheric pre-storm behaviour at the EIA region may better be understood if electric field and IMF-Bz are not significant. This assertion needs further studies by analyzing the ionospheric response during SSC period, which may further delineate the unresolved problem of ionospheric pre-storm phenomena. The inference on the synergy between the SSC and the main phase EIA structure is that plasma structure at the SSC period can foretell or trigger the EIA structure at the main phase (see Adekoya et al., 2012a; 2013; Adekoya and Adebesin, 2015). Further, the observed equatorial peak may be related to the impact of disorientation of particles in the foreshock region of the solar wind on the Earth magnetosphere (Mansilla

2007; Blagoveshchensky and Kalishin 2009; Danilov 2013; Adekoya et al., 2012a; Adekoya and Adebesin, 2015). That is, reduction in the equatorward wind flow gives rise to the poleward wind flow, hence, the plasma convergence at the equator which give rise to the TEC variation. Thereafter, as the storm gain momentum and releases more energy, the convective energy through the induced PPEF and storm-time equatorward wind reinforced, generate and extended EIA circulation in the ionosphere. This consequently enhances the TEC at either side of the equator and a monotonous decrease at the dip equator. At the recovery phase of the storm, the TEC experiences a gradual build-up structure of a forward plasma fountain effect, which becomes conspicuous on March 19 and gradually suppressed thereafter. There are two major orientations of storm-time equatorial electric fields, the eastward and westward zonal electric fields which are interpreted in terms of upward and downward plasma drift imposed either by PPEFs or DDEFs. The ionospheric disturbance dynamo is synonymous with the thermospheric disturbance processes at the recovery phase, which is caused by the thermospheric heating and long-duration electric field, and instigate the changes in the thermospheric circulation patterns at equatorial and low latitudes in the daytime (Blanc and Richmond, 1980). Also noted was that the TEC behaviour at nighttime periods is predominantly dominated by a weak forward plasma fountain. The TEC variations around these periods were insignificant. This weak plasma behaviour at nighttime may not necessarily be related to the disturbance neutral wind absorption that gives rise to the poleward wind alone, but with the presence of lower or insignificant zonal electric field perturbations due to the Coriolis force (Abdu et al., 2003; Tsurutani et al., 2014; Tulasi-Ram et al., 2016).

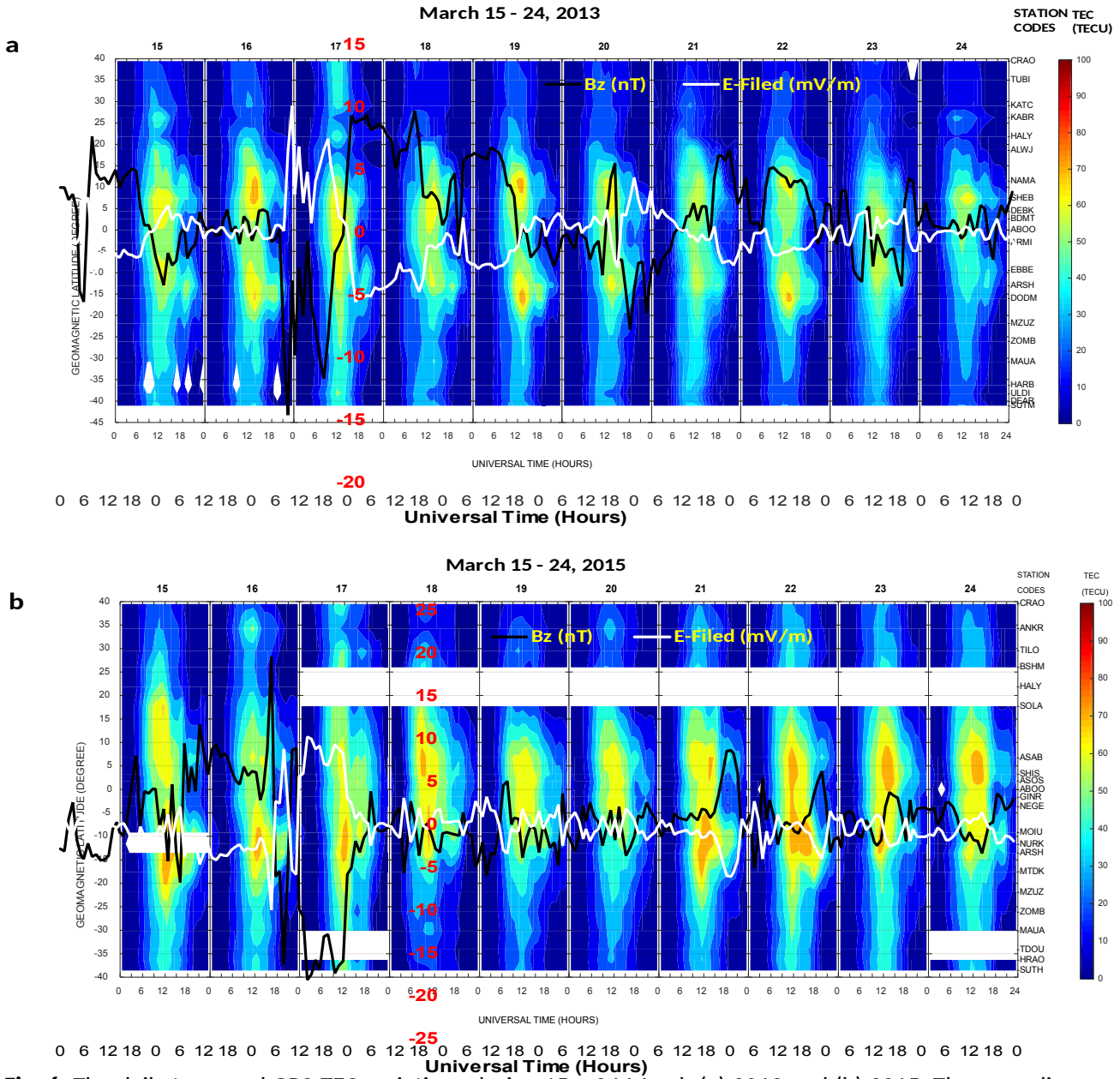

Fig. 6: The daily temporal GPS-TEC variations during 15 – 24 March (a) 2013 and (b) 2015. The curve lines are the interplanetary magnetic field (IMF-Bz) (black) and electric filed (white) are the expressions to observed the

changes in the low-latitude ionosphere due to the magnetospheric energy convection. The fields variation explains the effects of the different directions of the electric fields and IMF-Bz as it invoked the PPEF and DDEF effects that subsequently affect the ionospheric zonal electric field and vertical plasma drift (E x B drift).
Further, the plasma anomaly structures observed during the March 17, 2013 storm could be more intensified or dynamic if the strength of the magnetospheric convection energy increases. The Strom of March 17, 2015, was seen to be greater in dynamic and possesses more fields strength than that of March 2013. Consequently, the ionospheric plasma circulation was seen to be more variable and depicts a distinctive plasma structure during the storm's main and recovery phases respectively. On March 17, 2015, the ionospheric response appears to be more dynamic as the TEC variation on this day was significantly extended (Figure 6b). The TEC variation distinctively exhibits hemispheric asymmetry, which was more enhanced in the southern hemisphere. However, the hourly TEC behaviour showed reversed wave structures around 1700 – 1900 UT (1920 – 2120 LT), as the hemispheric enhancement is suppressed, which may be due to the reversed plasma fountain mechanisms (see Fig. 5). The reverse plasma fountain is a phenomenon that drives mainly by two possible mechanisms as hitherto noted, namely, rapidly induce PPEF and strong equatorward wind flow that imposed westward zonal electric field that aids the downward plasma motion of the ionosphere. It has been suggested that the westward electric field during the daytime could be related to the downward vertical plasma drifts (Adebesin et al., 2019; 2013a), which inhibited the forward plasma fountain effect. Again, on March 18, 2015, one could see a rapidly formed TEC enhancement at either side of the equator compared to that of March 2013 (Figure 6b). The fountain-like structure around this period might affirm the possibility that the wave structure was due to the long-lived disturbance dynamo electric fields (DDEF) due to the prevalence precipitation of energy stored in the high latitude as Joule heating to the lower latitude (Fejer, 2002; Blanc and Richmond, 1980), equatorward wind and the background storm-time ionospheric mechanisms, which strengthened and extended the EIA. These storm-time mechanisms as well influenced the development of positive and negative ionospheric storm in the EIA region through circulation. The weak EIA which was noted on March 19 and 20 (Figure 6b) could be related to the fact that the equatorward wind flow around these days has reduced, which subsequently affect the vertical plasma drift as the plasma transport is controlled by solar photoionization.

Therefore, figure 7 presents a clear description of these plasma structures and their fields dynamo effect during sudden storm commencement, magnetic disturbed and quiet periods. This figure described the role played by the induced magnetospheric energy on the zonal electric field in plasma distribution, which explains the response of the observed TEC variations. As deduced, the ionization anomaly is more variable when the field strength due to the intensified magnetospheric energy convection increased. Moreover, the fact that these two storms were driven by the same solar wind driver gas does not mean that their ionization composition/anomaly structure will be the same. What matters most is the rate of magnetospheric energy convection which is determined by the sunspot number, hence the difference in the Dst magnitudes. That is, an increase in the convective field strength will increase the dynamics structure of plasma/ionization anomaly and vice versa. Therefore, the observed strong EIA structures may be prompt from the enhanced field strength and circulation processes reinforced by the magnetospheric convection energy.

Another notable point is the observed changes in the hemispheric TEC variations between the storm of March 2013 and that of 2015. A critical view of the diurnal TEC variation revealed hemispheric asymmetry during the two storms. At the main phase of the storm of March 2013, the TEC variation was more enhanced in the northern hemisphere, this was overturned during the March 2015 storm. However, at the recovery phases of the storms, the TEC variation was hemispherically symmetry, the TEC variation was more accrued in the northern hemisphere than it appeared in the southern hemisphere. However, it should be noted that the hemispheric TEC variation at the recovery phase of the storm of March 2015 was more increased in strength and magnitude. The difference could be related to the rate at which magnetospheric convectional fields influenced the equatorward winds and thermospheric compositions (Astafyeva et al., 2015). Further, it was observed that the two storms were driven by the same driver gas, triggered by coronal mass ejections according to their interplanetary plasma sheath fields orientations. This eliminated any doubt of the seasonal anomaly and contribution of sheath field mechanisms. This points to the fact that the hemispheric response differs during different geomagnetic storms, as the strength of the ionospheric storm is determined by the rate of induced magnetospheric energy.

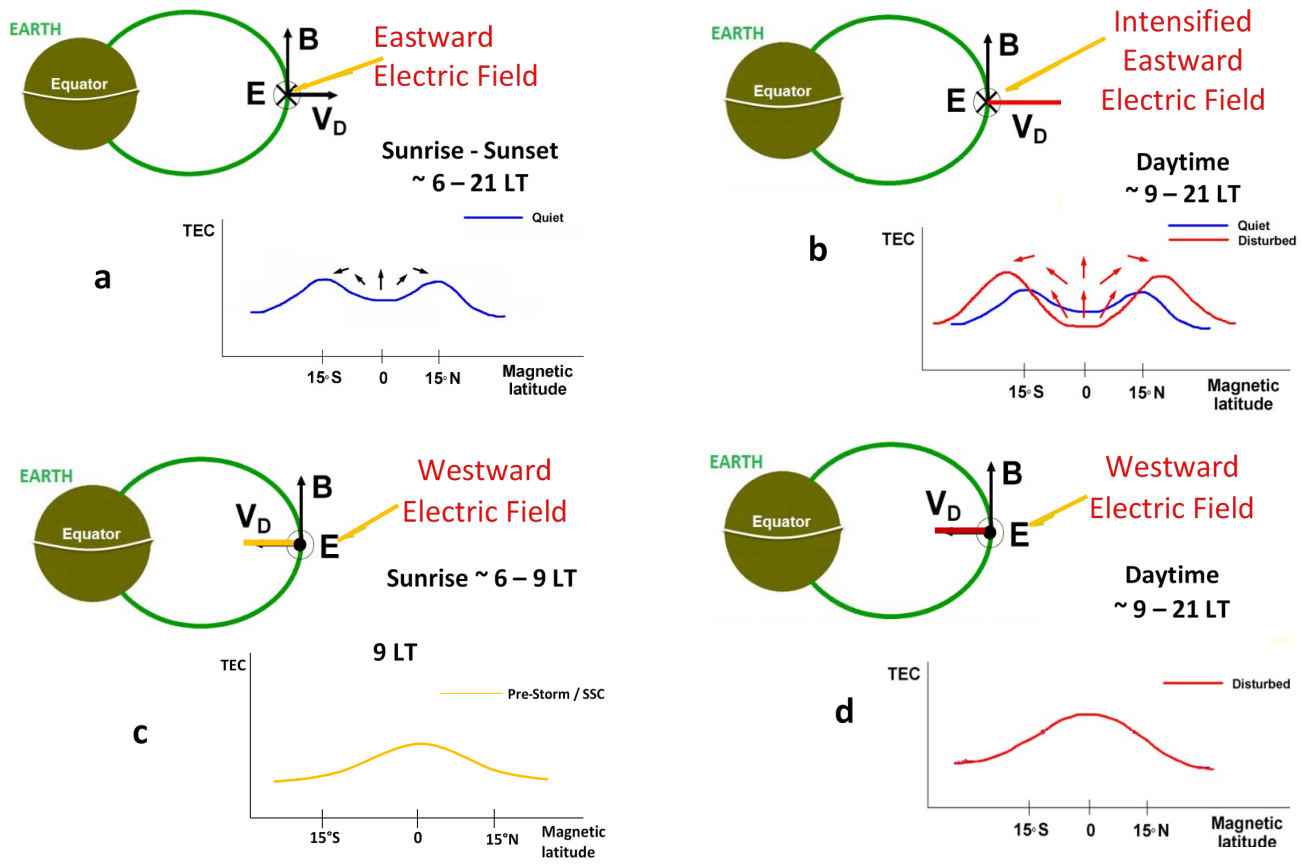

Fig. 7: The Plasma structure of the electrodynamic fields effect in response to the studied space weather events (a) the signature of a a quiet-time forward plasma fountain circulation on the ionosphere (weak EIA structure) (b) Signature of a disturbed strong EIA (c) Signature of a equatorial peak during sudden storm commencement (SSC)/ Pre-storm (Equatorial Peak) (d) Signature of a disturbed reversed plasma fountain due to great space weather event.

Acknowledgement

We acknowledge use of the African Geodetic Reference Frame (http://www.afrefdata.org) and International GNSS service (http://www.igs.org) for the GPS-TEC data. We thank the Scientists who maintain the various IGS site that ensure the continuous availability of GPS data. Also, we are grateful to the working team of the National Space Science Data Centres (NSSDC's) OMNI database (http://nssdc.gsfc.nasa.gov/omniweb) for the geomagnetic and interplanetary data.

References

Abdu, M. A. (1997), Major phenomena of the equatorial ionosphere-thermosphere system under disturbed conditions, J. Atmos. Sol. Terr. Phys., 59(13), 1505–1519, doi:10.1016/S1364-6826(96)00152-6.

Abdu, M. A., I. S. Batista, H. Takahashi, J. MacDougall, J. H. Sobral, A. F. Medeiros, and N. B. Trivedi (2003), Magnetospheric disturbance induced equatorial plasma bubble development and dynamics: A case study in Brazilian sector, J. Geophys. Res., 108 (A12), 1449, doi:10.1029/2002JA009721.

Adebesin, B. O., J. O. Adeniyi, I. A. Adimula, B. W. Reinisch, K. Yumoto (2013a), F2 layer characteristics and electrojet strength over an equatorial station, Advances in Space Research, 52 (5) 791 – 800 http://dx.doi.org/10.1016/j.asr.2013.05.025.

Adebesin, B. O., J. O. Adeniyi, I. A. Adimula, and B. W. Reinisch (2013b), Equatorial vertical plasma drift velocities and electron densities inferred from ground-based ionosonde measurements during low solar activity, J. Atmos. Sol. Terr. Phys., 97, 58–64, doi: 10.1016/j.jastp.2013.02.010.

Adebesin, B. O., B. J. Adekoya, and T. W. David (2019), Plasma transport process in the equatorial/low-latitude ionosphere, *Adv. Space Res.*, 63, 1619 - 1633, doi: 10.1016/j.asr.2018.11.013.

Adekoya, B. J., and B. O. Adebesin (2014), Hemispheric, seasonal and latitudinal dependence of storm-time ionosphere during low solar activity period, Advances in Space Research 54 (2014) 2184–2193, doi: 10.1016/j.asr.2014.08.013.

Adekoya, B. J., and B. O. Adebesin (2015), Ionospheric and Solar Wind Variation during Magnetic Storm Onset and Main Phase at Low- and Mid-latitudes, *Acta Geophysica* 63 (4) 1150-1180, doi: 10.1515/acgeo-2015-0020.

Adekoya, B. J., and V. U. Chukwuma (2016), Ionospheric F2 layer responses to total solar eclipses at low- and mid-latitude, J. Atmos. Sol. Terr. Phys., 138–139, 136–160, doi: 10.1016/j.jastp.2016.01.006.

Adekoya, B. J., and V. U. Chukwuma (2018), Classification and quantification of solar wind driver gases leading to intense geomagnetic storms, *Adv. Space Res.*, 61 (1), 274-286, doi: 10.1016/j.asr.2017.09.036.

Adekoya, B. J., V. U. Chukwuma, N. O. Bakare, and T. W. David (2012a), On the effects of geomagnetic storms and Pre-storm phenomena on low and middle latitude ionospheric F2, *Astrophys. Space Sci.*, 340 (2), 217–235. doi:10.1007/s10509-012-1082-x.

Adekoya, B. J., V. U. Chukwuma, N. O. Bakare, and T. W. David (2012b), Effects of geomagnetic storm on middle latitude ionospheric F2 variations during storm of April (2–6), 2004, *Indian J. Radio Sci. Space Phys.*, 41 (6), 606–616.

Adekoya, B.J., V. U. Chukwuma, and S. A. Salako, (2013), On the coexistence of positive and negative ionospheric storm during geomagnetic storms and pre-storm phenomena on low and low-mid latitude. In: Book of proceedings of 5th annual conference of the Nigeria union of radio science (NURS) an affiliate of International union of radio science Nigeria (URSI), 15–28. ISBN: 978-978-934-657-8.

Adekoya, B. J., V. U. Chukwuma, and B. W. Reinisch (2015), Ionospheric vertical plasma drift and electron density response during total solar eclipses at equatorial/low latitude, *J. Geophys. Res. Space Physics*, 120, 8066-8084, doi: 10.1002/2015JA021557

Amaechi, P. O., E. O. Oyeyemi, and A. O. Akala (2018), The response of African equatorial/low-latitude ionosphere to 2015 St. Patrick's Day geomagnetic storm. Space Weather, 16, 601–618, doi: 10.1029/2017SW001751

Amory-Mazaudier, C., O. S. Bolaji, and V. Doumbia (2017), On the historical origins of the CEJ, DP2, and Ddyn current systems and their roles in the predictions of ionospheric responses to geomagnetic storms at equatorial latitudes, J. Geophys. Res. Space Physics, 122, 7827–7833, doi: 10.1002/2017JA024132.

Astafyeva, E., I. Zakharenkova, & M. Förster (2015), Ionospheric response to the 2015 St. Patrick's Day storm: A global multi-instrumental overview, J. Geophys. Res. Space Physics, 120, 9023–9037, doi:10.1002/2015JA021629.

Astafyeva, E., I. Zakharenkova, K. Hozumi, P. Alken, P. Coïsson, M. R. Hairston, and W. R. Coley (2018), Study of the equatorial and low-latitude electrodynamic and ionospheric disturbances during the 22–23 June 2015 geomagnetic storm using ground-based and spaceborne techniques, *J. Geophys. Res. Space Physics*, 123, 2424–2440, doi: 10.1002/2017JA024981.

Bagiya, M. S., Sunil, A.S., Chakrabarty, D., Sunda, S., (2017). Salient features of the dayside low latitude ionosphere response to the main phase step-I of the 17 March 2015 geomagnetic storm. Adv. Space Res. 60, 1827–1837.

Balan, N., and G. J. Bailey (1995), Equatorial plasma fountain and its effects: Possibility of an additional layer. Journal of Geophysical Research: Space Physics, 100 (A11), 21421–21432, doi:10.1029/95ja01555.

Balan, N., K. Shiokawa, Y. Otsuka, S. Watanabe, and G. J. Bailey (2009a), Super plasma fountain and equatorial ionization anomaly during penetration electric field, J. Geophys. Res., 114, A03310, doi:10.1029/2008JA013768.

Balan, N., H. Alleyne, Y. Otsuka, D. Vijaya Lekshmi, B. G. Fejer and I. McCrea (2009b), Relative effects of electric field and neutral wind on positive ionospheric storms, Earth Planet Space, 60, 1–7.

Balan, N., Y. Otsuka, M. Nishioka, J. Y. Liu, and G. J. Bailey (2013), Physical mechanisms of the ionospheric storms at equatorial and higher latitudes during the recovery phase of geomagnetic storms, *J. Geophys. Res. Space Physics*, 118, 2660-2669, doi: 10.1002/jgra.50275.

Balan, N., J. Souza, G.J. Bailey (2017), Recent developments in the understanding of equatorial ionization anomaly: A review, Journal of Atmospheric and Solar-Terrestrial Physics, 171 (), 3 - 11, doi: 10.1016/j.jastp.2017.06.020.

Balan N., Liu L. B., and Le H. J. (2018), A brief review of equatorial ionization anomaly and ionospheric irregularities, *Earth Planet. Phys.*, 2 (4), 1 - 19. http://doi.org/10.26464/epp2018025

Baumjohann, W. (1982). Ionospheric and field-aligned current systems in the auroral zone: a concise review. Advances in Space Research, 2(10), 55–62. doi: 10.1016/0273-1177(82)90363-5

Blagoveshchensky, D.V., and A. S. Kalishin (2009), Increase in the critical frequency of the ionospheric F region prior to the substorm expansion phase, Geomagn. Aeronom. 49 (2), 200–209.

Blanc, M., and A. D. Richmond (1980), The ionospheric disturbance dynamo, J. Geophys. Res., 85, 1669–1686, doi:10.1029/JA085iA04p01669.

Bolaji, O., O. Owolabi, E. Falayi, E. Jimoh, A. Kotoye, O. Odeyemi, B. Rabiu, P. Doherty, E. Yizengaw, Y. Yamazaki, J. Adeniyi, R. Kaka, and K. Onanuga (2017), Observations of equatorial ionization anomaly over Africa and Middle East during a year of deep minimum, Ann. Geophys., 35, 123-132, doi: 10.5194/angeo-35-123-2017.

Dabas, R. S., Bhuyan, P. K., Tyagi, T. R., Bhardwaj, R. J., Lal, J. B. (1984), Day-to-day changes in ionospheric electron content at low latitudes. Radio Sci., 19, 749 – 756.

Danilov, A. D. (2013), Ionospheric F-region response to geomagnetic disturbances, Adv. Space Res., 52 (3), 343-366, doi:10.1016/j.asr.2013.04.019.

Echer, E., Gonzalez, W. D., Tsurutani, B. T., (2008) Interplanetary conditions leading to superintense geomagnetic storms (Dst ≤ −250 nT) during solar cycle 23. Geophys. Res. Lett., 35 (6), L06S03, doi: 10.1029/2007GL031755.

Fagundes, P. R., F. A. Cardoso, B. G. Fejer, K. Venkatesh, B. A. G. Ribeiro, and V. G. Pillat (2016), Positive and negative GPS-TEC ionospheric storm effects during the extreme space weather event of March 2015 over the Brazilian sector, *J. Geophys. Res. Space Physics*, 121, 5613–5625, doi: 10.1002/2015JA022214.

Fejer, B.G. (1981), The equatorial ionospheric electric fields. A review. J. Atmos. Terr. Phys., 43, 377–386.

Fejer, B. G. (1997), The electrodynamics of the low-latitude ionosphere: recent results and future Challenges, J. Atmos. Sol. Terr. Phys., 59 (13), 1465–1482.

Fejer, B. G. (2002), Low latitude storm time ionospheric electrodynamics, J. Atmos. Sol. Terr. Phys., 64, 1401–1408.

Fejer, B. G. (2011), Low latitude ionospheric electrodynamics, Space Sci. Rev. 158, 145 – 166, doi:10.1007/s11214-010-9690-7.

Gonzalez, W. D., B. Tsurutani, and A. L. C. Gonzalez, (1999), Interplanetary origin of geomagnetic storms, *Space Sci. Rev*. 88, 529-562.

Gonzalez, W. D., Clua de Gonzalez, A. L., Sobral, J. H. A., Dal Lago, A., Vieira, L. E. (2001), Solar and interplanetary causes of very intense storms, J. Atmos. Sol-Terr. Phys., 63, 403–412.

Horvath, I., and B. C. Lovell (2008), Formation and evolution of the ionospheric plasma density shoulder and its relationship to the superfountain effects investigated during the 6 November 2001 great storm, *J. Geophys. Res.*, 113, A12315, doi:10.1029/2008JA013153.

Ikubanni, S. O., S. J. Adebiyi, B. O. Adebesin, K. O. Dopamu, B. W. Joshua, O. S. Bolaji, and B. J. Adekoya, (2018), Response of GPS-TEC in the African Equatorial Region to the Two Recent St. Patrick‟s Day Storms, International Journal of Civil Engineering and Technology, 9 (10), 1773–1790.

Kamide, Y. (1982), The relationship between field-aligned currents and the auroral electrojets: a review, Space Science Reviews, 31, 127-243.

Kelley, M. C., B. G. Fejer, and C. A. Gonzales (1979), An explanation for anomalous equatorial ionospheric electric field associated with a northward turning of the interplanetary magnetic field, Geophys. Res. Lett., 6 (4), 301.

Kelley, M. C., J. J. Makela, J. L. Chau, and M. J. Nicolls (2003), Penetration of the solar wind electric field into the magnetosphere/ionosphere system, Geophys. Res. Lett., 30 (4),1158, doi:10.1029/2002GL016321.

Le-Huy, M., and C. Amory-Mazaudier (2005), Magnetic signature of the ionospheric disturbance dynamo at equatorial latitudes, “Ddyn”, *J. Geophys. Res.*, 10, A10301, doi:10.1029/2004JA010578.

Liu, L., Chen, Y., Le, H., Kurkin, V. I., Polekh, N. M., & Lee, C.-C. (2011). The ionosphere under extremely prolonged low solar activity. Journal of Geophysical Research, 116, A04320. https://doi.org/10.1029/2010JA016296

Malandraki, O. E. and N. B. Crosby (2018), Solar Energetic Particles and SpaceWeather: Science and Applications, in Solar Particle Radiation Storms Forecasting and Analysis, The HESPERIA HORIZON 2020 Project and Beyond, Malandraki, O. E. and N. B. Crosby (eds.), Astrophysics and Space Science Library 444, pg 19, doi: 10.1007/978-3-319-60051-2_1

Mansilla, G. A. (2007), Ionospheric effects of an intense geomagnetic storm, Studia Geophys. Geodet., 51 (4), 563–574.

Mansilla, G. A. (2019). Ionospheric disturbances at low and mid-low latitudes of the South American sector during the March 2015 great storm. *Advances in Space Research* 63 (2019) 3545–3557

Mendillo, M. (2006), Storms in the ionosphere: Patterns and processes for total electron content, Rev. Geophys.,44, RG4001, doi:10.1029/2005RG000193.

Namgaladze, A. A., Förster, M., Yurik, R. Y., (2000), Analysis of the positive ionospheric response to a moderate geomagnetic storm using a global numerical model, Ann. Geophys. 18, 461–477.

Nava, B., J. Rodríguez-Zuluaga, K. Alazo-Cuartas, A. Kashcheyev, Y. Migoya-Orué, S. M. Radicella, C. Amory-Mazaudier, and R. Fleury (2016), Middle- and low-latitude ionosphere response to 2015 St. Patrick’s Day geomagnetic storm, J. Geophys. Res. Space Physics, 121, 3421–3438, doi:10.1002/2015JA022299.

Oluwadare, T. S., C. N. Thai, A. O. Akala, S. Heise, M. Alizadeh, and H. Schuh, (2018), Characterization of GPS-TEC over African equatorial ionization anomaly (EIA) region during 2009–2016, Adv. Space Res., 63 (1), 282 - 301, doi: 10.1016/j.asr.2018.08.044.

Prölss, G. W. (1995), Ionospheric F region storms, in Handbook of Atmospheric Electrodynamics, edited by H. Volland p.195–248, CRCPress, Boca Raton

Ramsingh, S. Sripathi, S. Sreekumar, S. Banola, K. Emperumal, P. Tiwari, and B. S. Kumar (2015), Low-latitude ionosphere response to super geomagnetic storm of 17–18 March 2015: Results from a chain of ground-based observations over Indian sector, J. Geophys. Res. Space Physics, 120, 10,864–10,882, doi:10.1002/2015JA021509.

Rishbeth, H. (1998), How the thermospheric circulation affects the ionospheric F2-layer, J. Atmos. Terr. Phys., 60, 1385–1402.

Rishbeth, H., A. J. Lyon, and M. Peart (1963), Diffusion in the equatorial F layer. J. Geophys. Res., 68 (9), 2559 - 2569, doi: 10.1029/JZ068i009p02559.

Rishbeth, H., & M. Mendillo (2001), Patterns of F2-layer variability, *J. Atmos. Sol. Terr. Phys*., 63, 1661-1680.

Tulasi Ram, S., T. Yokoyama, Y. Otsuka, K. Shiokawa, S. Sripathi, B. Veenadhari, R. Heelis, K. K. Ajith, V. S. Gowtam, S. Gurubaran, P. Supnithi, and M. Le Huy (2016), Duskside enhancement of equatorial zonal electric field response to convection electric fields during the St. Patrick's day storm on 17 March 2015, J. Geophys. Res. Space Physics, 121, 538–548, doi:10.1002/2015JA021932.

Tsurutani, B., A. Mannucci, B. Iijima, M. A. Abdu, J. A. Sobral, W. Gonzalez, F. Guarnieri, T. Tsuda, A. Saito, K. Yumoto, B. Fejer, T. J. Fuller-Rowell, J. Kozyra, J. C. Foster, A. Coster and V. M. Vasyliunas (2004), Global dayside ionospheric uplift and enhancement associated with interplanetary electric fields, *J. Geophys. Res.*, 109, A08302, doi:10.1029/2003JA010342.

Tsurutani, B. T., O. P. Verkhoglyadova, A. J. Mannucci, A. Saito, T. Araki, K. Yumoto, T. Tsuda, M. A. Abdu, J. H. A. Sobral, W. D. Gonzalez, H. McCreadie, G. S. Lakhina, and V. M. Vasyliunas (2008), Prompt penetration electric fields (PPEFs) and their ionospheric effects during the great magnetic storm of 30–31 October 2003, *J. Geophys. Res.*, 113, A05311, doi:10.1029/2007JA012879

Tsurutani B. T., E. Echer, K. Shibata, O. P. Verkhoglyadova, A. J. Mannucci, W. D. Gonzalez, J. U. Kozyra, M. Pätzold (2014), The interplanetary causes of geomagnetic activity during the 7–17 March 2012 interval: a CAWSES II overview, J. Space Weather Space Clim., 4 (A02). doi:10.1051/swsc/2013056.

Venkatesh, K., S. Tulasi Ram, P. R. Fagundes, G. K. Seemala, and I. S. Batista (2017), Electrodynamic disturbances in the Brazilian equatorial and low-latitude ionosphere on St. Patrick's Day storm of 17 March 2015, *J. Geophys. Res. Space Physics*, 122, doi:10.1002/2017JA024009.

Vijaya Lekshmi, D., N. Balan, V. K. Vaidyan, H. Alleyne, and G. J. Bailey (2007), Response of the ionosphere to super storms, J. Adv. Space Res., 41 (4), 548-555, doi: 10.1016/j.asr.2007.08.029.

Wang, W., J. Lei, A. G. Burns, S. C. Solomon, M. Wiltberger, J. Xu, Y. Zhang, L. Paxton, and A. Coster (2010), Ionospheric response to the initial phase of geomagnetic storms: Common features, J. Geophys. Res., 115, A07321,
doi:10.1029/2009JA014461.

Wei, Y., B. Zhao, G. Guozhu, and W. Wan (2015), Electric field penetration into Earth's ionosphere: A brief review for 2000–2013, Sci. Bull., 60(8), 748–761, doi:10.1007/s11434-015-0749-4.

Williams, E. R., and G. Sátori (2007), Solar radiation-induced changes in ionospheric height and the Schumann resonance waveguide on different timescales, Radio Sci.,42, RS2S11, doi:10.1029/2006RS003494

Yizengaw, E., P. Doherty, and T. Fuller-Rowell (2013), Is Space Weather Different Over Africa, and If So, Why? AGU Chapman Conference Report, Space Weather, 11, doi:10.1002/swe.20063.